Preprint Cambridge Centre for Computational Chemical Engineering ISSN 1473 – 4273

Detailed Population Balance Modelling of TiO_2 Synthesis in an Industrial Reactor

Astrid Boje[1], Jethro Akroyd[1],
Stephen Sutcliffe[3], John Edwards[3], Markus Kraft[1,2]

released: 1 December 2016

[1] Department of Chemical Engineering
and Biotechnology
University of Cambridge
New Museums Site
Pembroke Street
Cambridge, CB2 3RA
United Kingdom
E-mail: mk306@cam.ac.uk

[2] School of Chemical and
Biomedical Engineering
Nanyang Technological University
62 Nanyang Drive
Singapore, 637459

[3] Huntsman Pigments and Additives
Titanium House
Hanzard Drive
Wynyard Park, TS22 5FD
United Kingdom

Preprint No. 176

Keywords: titanium dioxide, ideal reactor, network, particle model, stochastic, population balance

Edited by
Computational Modelling Group
Department of Chemical Engineering and Biotechnology
University of Cambridge
New Museums Site
Pembroke Street
Cambridge CB2 3RA
United Kingdom

Fax: + 44 (0)1223 334796
E-Mail: c4e@cam.ac.uk
World Wide Web: http://como.cheng.cam.ac.uk/

Highlights

- An industrial titania reactor is modelled
- A reactor network is used to describe localised flow, composition and temperature
- A multivariate particle description is used, enabling characteristics of particle shape and size to be explored in detail
- A short process parameter study is performed, demonstrating the potential to investigate the effect of operational choices on product characteristics.

Abstract

This paper uses a network of ideal flow reactors and a detailed population balance model to study the evolution of the size and shape distributions of pigmentary titanium dioxide, formed under industrial synthesis conditions. The industrial reactor has multiple reactant injections, a tubular working zone in which the exothermic reaction is completed, and a cooling zone. A network of continuously stirred tank reactors (CSTRs) is used to model variation in composition around the feeds and plug flow reactors (PFRs) with prescribed temperature gradients are used to describe the working and cooling zones. The quality of the industrial product depends on its morphology, and this is influenced by factors including temperature and throughput. In this paper, a multivariate particle model is accommodated using a stochastic method and the particle morphology is characterized in terms of the distributions of primary and aggregate particle diameters, number of primary particles per particle and neck radii of connected primary particles. Increasing temperature or residence time is shown to produce larger particles. Qualitative similarities are highlighted between such findings and previous studies. The throughput studies are also in qualitative agreement with empirical industrial experience. There is scope for extending and improving the current model; however, it is suggested that insights of this type could be used to inform the design and operation of the industrial process.

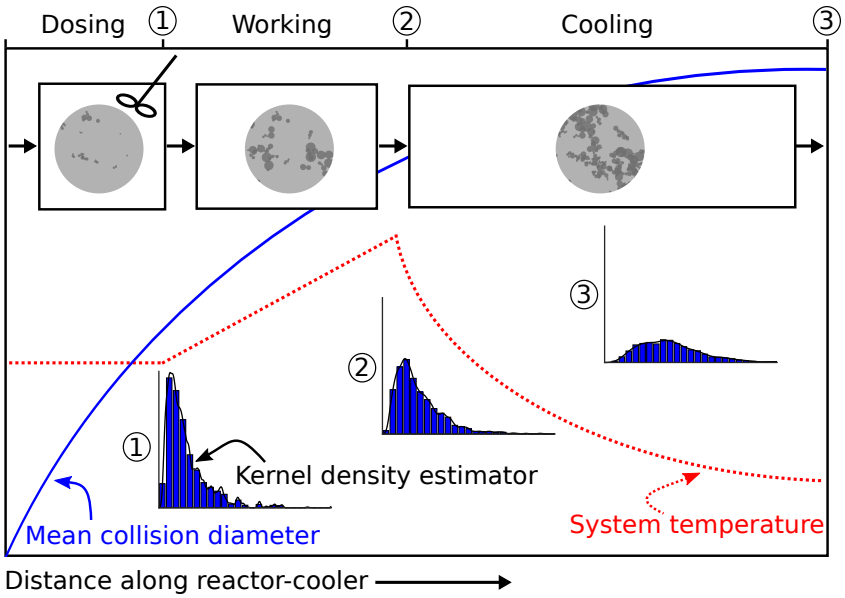

Contents

1 Introduction

Titanium dioxide (TiO_2, titania) powder is used ubiquitously in pigments, as well as in cosmetics, pharmaceuticals, ceramics and catalysts. It can be synthesised by the oxidation of titanium tetrachloride ($TiCl_4$) in either a flame, or by stage-wise addition to a plasma [3, 15]. The TiO_2-forming reaction has the overall stoichiometry:

$$TiCl_4 + O_2 \rightarrow TiO_{2(\text{particles})} + 2Cl_2.$$

The optical properties of the product are determined by the particle size and morphology. For example, the tint depends on the particle size distribution (PSD); and the crystal phase determines the magnitude of the refractive index and the photocatalytic nature [7, 20, 48]. The use of this reaction in titanium dioxide pigment manufacture necessitates milling of the particles in order to achieve the necessary size and distribution for light scattering. Milling has a significant impact on the energy cost of the product; thus, ease of milling can be an important consideration.

Many factors influence the size and morphology of the particles, including the gas-phase reaction rates, particle processes, operating conditions, type of plasma-forming gas, reactor configuration and use of chemical additives. Park and Park [33] discuss the role of these different factors and summarise the difficulties inherent in understanding and controlling the synthesis process.

Reactors for the industrial synthesis of titanium dioxide often have multiple feed points, with independently controlled feed rates and pre-heat temperatures [48]. The operating conditions include temperatures in the range 1000-1500 K, pressures of up to 4.5 bar and residence times in the milliseconds. This limits the availability of industrially relevant studies; thus most published experimental work is under milder laboratory-scale and flame synthesis conditions. Laboratory-scale synthesis in different plasmas at atmospheric pressure was investigated by Kartaev et al. [20]; and Garrick and Wang [14], George et al. [16], Hong et al. [19], Tsantilis et al. [46] considered particle growth in a flame reactors.

These studies are important – for example, the thin film studies of Ghoshtagore [17] and the hot wall reactor of Pratsinis et al. [40] have provided insights into the kinetics of the overall oxidation reaction. However, the rates of the particle growth processes are significantly different under industrial conditions. For instance, a study by Pratsinis and Spicer [39] found that surface growth was only significant at high $TiCl_4$ concentrations. In the absence of published experimental data for the industrial synthesis, it is useful to compare the available literature to numerical studies under the harsher conditions used in the industrial process. This paper provides a means towards this aim.

Numerical studies of titania synthesis generally involve a population balance model that accounts for processes such as nucleation, coagulation, surface reaction and sintering. A concise review of the processes and common numerical methods can be found in Kraft [23]. This model is typically solved using monodisperse [22, 24, 39, 44], moment [3, 13], sectional [45, 50, 51] or finite element [4] methods. These techniques are popular because they give a set of differential equations for the particle dynamics that can be solved with the chemistry and flow. However, the limitation of these methods is that they require the description of each particle to remain relatively simple. Particles are typically spherical

and are only described by a measure of their size, or of their size and volume.

The treatment of the particle processes is constrained by the level of detail inherent in the model. For example, in a spherical model, collisions must result in perfect coalescence [39]. Menz and Kraft [28] found that incorporating more detail about the particles was particularly important for cases where coagulation and sintering occur on different time scales, or where the coagulating particles are highly polydisperse.

In this work, a stochastic method is used to resolve fully the particle structure beyond the extent that is possible using monodisperse, moment or sectional methods. This information is believed to be important here because it directly relates to the optical properties of the final product, as well as the energy requirement of the milling step in the industrial process. Stochastic numerical methods simulate particle processes as discrete events occurring on computational particles in a representative sample of the population. Stochastic population balance modelling has been used to simulate formation of soot [6], silica [42] and titania [2, 48]. Yapp et al. [53] used a detailed population balance to compute the optical band gap of polycyclic aromatic hydrocarbons in an ethylene diffusion flame. Menz et al. [29] used a stochastic method to investigate the synthesis of silicon nanoparticles, using a network of ideal reactors to describe flow behaviour in the reactor.

Computational fluid dynamics (CFD) simulations have been used to model the flow fields in titania synthesis in laboratory-scale plasma-chemical reactors [20], flame reactors [26, 52] and industrially representative reactors [3]. The non-ideal flow patterns observed suggest that treatment of flow is an important consideration for a model of the industrial system; however, the computational cost of solving the flow with CFD limits the complexity of the chemistry and particle models that can be used.

The equivalent reactor network (ERN) approach couples together ideal reactors such as continuously stirred tank reactors (CSTRs) and plug flow reactors (PFRs) to approximate the flow behaviour observed experimentally or by CFD. This has been used to simplify the treatment of turbulent reacting flows in models for particle synthesis so that an acceptable level of detail can be obtained in the chemistry and particle models [5, 26, 27, 31, 32].

The **purpose of this paper** is to demonstrate the potential to simulate the synthesis of TiO_2 in an industrial reactor, using a network of ideal reactors to account for variation in composition, temperature, and localised mixing. A linear network of CSTRs and PFRs is used to model an industrial reactor. A detailed population balance model is employed to obtain information about particle properties, such as size and morphology, which determine the product quality. The model is also applied to investigate different process conditions, which could be useful for predicting the effect of process phenomena such as temperature hot-spots on the product properties.

The **structure of this paper** is as follows: Section 2 discusses the particle model and processes, and gives a brief overview of the numerical methods used. Section 3 introduces the reactor network model and describes the base case operating conditions. Section 4.1 presents the results of the base case simulation and discusses related numerical considerations. Section 4.2 presents a short sensitivity study for reactor temperature, configuration and throughput, mentioning relevant literature studies and industrial experience. Finally, the current work is summarised in Section 5, along with suggestions for future work.

2 Model and methods

This work uses coupled solvers for the gas-phase chemistry and particle population balance. The chemical mechanism proposed by West et al. [49] is used for the gas-phase. It includes 28 gas-phase species, one solid species and 66 gas-phase reactions. A multivariate particle model is used and the population balance, which describes the formation and growth of particulate titania, is solved using a stochastic method to accommodate this.

2.1 Particle model

The simulated system is comprised of computational particles P_i, $i = 1,\ldots,N \leq N^{(\max)}$, in a sample volume V_{smp} (**Figure 1**). Each computational particle represents a certain number of physical particles and the sample volume defines the scaling between the physical system and the simulated system. The user-defined upper limit on the number of computational particles in the simulation is given by $N^{(\max)}$.

Each particle P_i is an aggregate structure which is described by a list of its constituent primary particles, and resolves the connectivity and degree of sintering between neighbouring primary particles [28, 53]. Let P_i have n_i primary particles p_j, $j = 1,\ldots,n_i$; and let the connectivity and shared surface area data be contained in $\mathbf{C}$ [41, 42]:

$$P_i = (p_1,\ldots,p_{n_i},\mathbf{C}).$$

Each primary particle p_j is defined in terms of the number, $\eta \in \mathbb{N}_0$, of titanium, oxygen and chlorine atoms it contains:

$$p_j = (\eta_{\text{Ti}},\eta_{\text{O}},\eta_{\text{Cl}}).$$

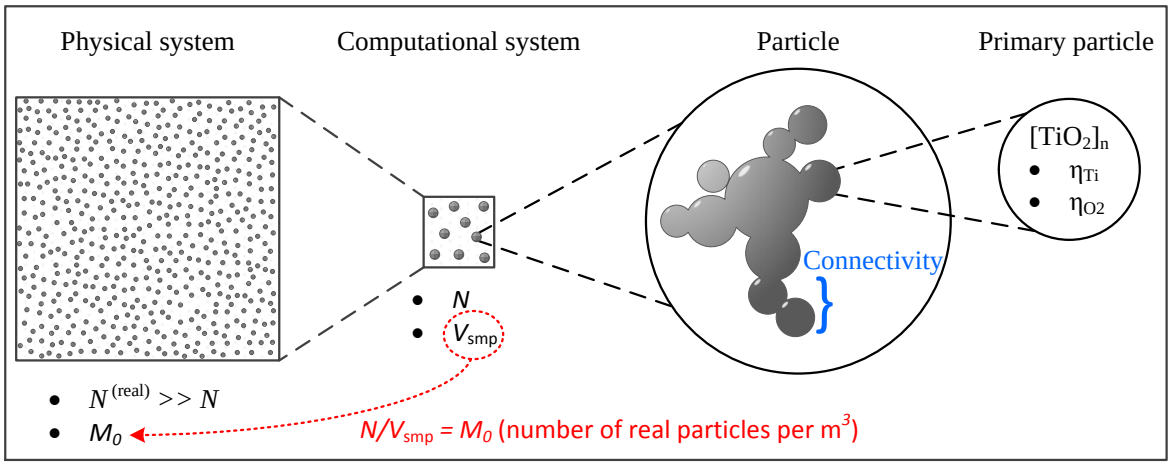

Figure 1: *Scaling of the physical system to a computational system, with N particles, contained within the sample volume V_{smp}, and primary particle connectivity and composition within each computational particle.*

The primary particle p_j has volume $v(p_j)$ and its diameter, d_p, is given by Equation (1).

$$d_\mathrm{p}(p_j) = \left(\frac{6v(p_j)}{\pi}\right)^{\frac{1}{3}} \tag{1}$$

The collision diameter, d_c, of each particle is computed from the total particle volume, V_i, and area, A_i, assuming a fractal dimension of 1.8 as discussed in Sander et al. [41] and Tsantilis et al. [46]. Constant/variable fractal dimensions are studied in Goudeli et al. [18]. Expressions for the collision diameter are compared in Patterson and Kraft [36]. It has been suggested that the specific choice of metric for approximation of aggregate structure does not have a significant effect relative to the current understanding of the formation and growth processes [36, 46].

$$d_\mathrm{c}(P_i) = \frac{6V_i}{A_i} n_i^{\frac{1}{1.8}} \tag{2}$$

The theoretical convergence as $N^{(\max)} \to \infty$ has been studied by Eibeck and Wagner [11], Patterson [34, 35] and Wells [47].

2.2 Particle processes

The processes governing formation and growth of particle in the population balance model include inception, surface growth, coagulation and sintering (**Figure 2**). These processes act on (pairs of) primary particles or whole particle aggregates as highlighted in Sections 2.2.1-2.2.4. The whole aggregate structure is available due to use of the multivariate particle model.

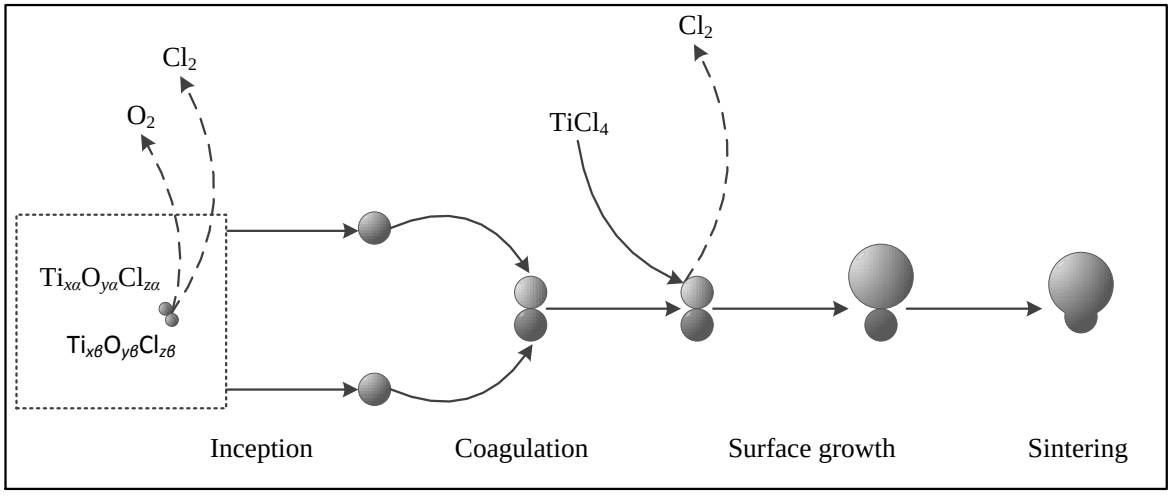

Figure 2: *Particle formation and growth processes.*

2.2.1 Inception

Inception refers to the nucleation of primary particles from precursor gas-phase species. Here, possible particle inception reactions are defined by a set of 105 bimolecular collisions between the various titanium oxychloride species ($Ti_xO_yCl_z$, $x,y,z \geq 1$) that are generated by the gas-phase mechanism, and the collision rate is determined by a transition regime coagulation kernel, with a molecular collision diameter of 0.65 nm [3, 6, 41, 48]. The inception reactions have the form:

$$Ti_{x_\alpha}O_{y_\alpha}Cl_{z_\alpha} + Ti_{x_\beta}O_{y_\beta}Cl_{z_\beta} \rightarrow (x_\alpha + x_\beta)\,TiO_{2_{(s)}} + \left(\frac{y_\alpha + y_\beta}{2} - x_\alpha - x_\beta\right)O_2 + \left(\frac{z_\alpha + z_\beta}{2}\right)Cl_2.$$

2.2.2 Surface reaction

Primary particles can undergo growth due to surface reaction with gaseous species. Here, the heterogeneous surface reaction is assumed to be first order in $TiCl_4$ and O_2, as in Akroyd et al. [3]. Equation (3) gives the growth rate, where k_s has Arrhenius form as in Equation (4), and A refers to the surface area per unit volume of the particle population. Values for the parameters k_1 and E_a were obtained by fitting the data from the experiment of Pratsinis et al. [40]: $k_1 = 1.34 \times 10^3$ m/s·m^3/mol and $E_a = 60$ kJ/mol.

$$\frac{d\left[TiO_2\right]}{dt} = k_s A \left[TiCl_4\right]\left[O_2\right] \tag{3}$$

$$k_s = k_1 \exp\left(-\frac{E_a}{RT}\right) \frac{\text{m}}{\text{s}} \cdot \frac{\text{m}^3}{\text{mol}} \tag{4}$$

2.2.3 Coagulation

Coagulation between particles P_i and P_j involves collision and lasting point contact, and is governed by the Smoluchowski equation [10]. The rate is described by the transition regime coagulation kernel K_{tr}, which is calculated as half the harmonic mean of the slip flow and free molecular kernels, K_{sf} and K_{fm} as in Equations (5)-(7), in which m is the particle mass, k_B is the Boltzmann constant, P is the pressure, and Kn is given by Equation (8) [42].

$$K_{tr} = \frac{K_{sf}K_{fm}}{K_{sf} + K_{fm}} \tag{5}$$

$$K_{sf}(P_i, P_j) = \frac{2k_B T}{3\mu}\left(\frac{1 + 1.257\text{Kn}(P_i)}{d_c(P_i)} + \frac{1 + 1.257\text{Kn}(P_j)}{d_c(P_j)}\right)\left(d_c(P_i) + d_c(P_j)\right) \tag{6}$$

$$K_{fm}(P_i, P_j) = 2.2\sqrt{\frac{\pi k_B T}{2}\left(\frac{1}{m(P_i)} + \frac{1}{m(P_j)}\right)}\left(d_c(P_i) + d_c(P_j)\right)^2 \tag{7}$$

$$\text{Kn}(P_i) = 4.74 \times 10^{-8}\frac{T}{P d_c(P_i)} \tag{8}$$

2.2.4 Sintering

Particle rounding occurs due to sintering; which is modelled between neighbouring pairs of primary particles p_i and p_j. As in other work [48, 51], it is assumed that the excess radius over that of a mass-equivalent spherical particle decays exponentially. Thus, the change in the common particle surface area, $A_{i,j}$, due to sintering is given by Equation (9), in which $A_{i,j}^{\text{sph}}$ is the surface area of a mass-equivalent spherical particle.

$$\frac{dA_{i,j}}{dt} = -\frac{1}{\tau_c}\left(A_{i,j} - A_{i,j}^{\text{sph}}\right) \tag{9}$$

The characteristic sintering time, τ_c, is given by Equation (10), in which $d_{i,j}$ is the minimum diameter of the two primaries. The expression was proposed by Kobata et al. [21] and derives from TiO_2 particles sintering through grain-boundary diffusion. This approach was used by West et al. [48]. Alternate expressions for τ_c are available [33].

$$\tau_c = 7.4 \times 10^8 T d_{i,j}^4 \exp\left(\frac{3.1 \times 10^4}{T}\right) \tag{10}$$

The sintering level, $s_{i,j}$ between the primary particle pair is given by Equation (11), as in Shekar et al. [42]. This describes the extent to which sintering has occurred, where $s_{i,j} = 0$ implies that the particles are in point contact and $s_{i,j} = 1$ implies that the primaries have coalesced to form a new particle [53]. Intermediate levels, $s_{i,j} \in (0,1)$, describe partially sintered particles, connected by a 'neck' of non-zero radius, and ability to describe such connections is believed to be one of the advantages of a multivariate particle model.

$$s_{i,j} = \frac{\frac{A_{i,j}^{\text{sph}}}{A_{i,j}} - 2^{-1/3}}{1 - 2^{-1/3}} \tag{11}$$

2.3 Numerical methods

The coupling between the gas-phase and particle systems is treated using an operator-splitting technique [6]. The gas-phase reactions are handled using an ordinary differential equation solver and the population balance is solved using either a direct simulation algorithm (DSA) or a stochastic weighted algorithm (SWA) [38, 42]. The reactors in the network are solved sequentially at each time step [29]. See Appendix B for the algorithms.

In the population balance solver, inflow, inception, coagulation and surface growth are modelled as stochastic processes and outflow and sintering are modelled as continuous processes. Continuous outflow is used to minimise propagation of error as recommended by Menz et al. [29] and is achieved by rescaling the sample volume. The waiting time between events is assumed to be exponentially distributed and the mean of the distribution is specified by the overall process rate for the current state. The probability of selecting a particular process is given by the ratio of the individual and overall process rates.

The DSA assigns equal statistical weights to each computational particle in the ensemble. That is, each computational particle represents the same number of physical particles.

This means that coagulation events deplete the sample, because each event combines two of the computational particles. In SWA, particles are given unequal weights. When a coagulation occurs, one of the two particles involved is left unaltered, and the other particle is updated to have the properties of the particle that would result from the coagulation event. This is accounted for by changing the weight of the updated particle as described elsewhere [38]. This improves the resolution of rare/large particles and can be useful for variance reduction in systems in which coagulation occurs to a large extent.

In order to improve computational efficiency, a linear process deferment algorithm [37] is implemented for surface growth. A majorant technique [9, 38] is used for computing the coagulation kernel and performing coagulation events. A binary tree data structure is used to store the particle lists, providing an efficient means of selecting particles based on a specific property [37].

3 Reactor model

The industrially representative titania reactor considered in this work (**Figure 3**) has two distinct zones. In the dosing zone (the shaded part), high temperature oxygen enters at $x = 0$, and gaseous $TiCl_4$ and O_2 are fed through the wall at three subsequent points. The second part of the reactor is called the working zone. Here, the gas-phase reactions continue to completion and the particulate product undergoes further growth. A qualitative temperature profile is shown in the lower half of Figure 3. The temperature does not increase significantly in the dosing zone due to the effect of the reactant injections through the reactor wall. The temperature increases across the working zone due to the exothermic oxidation reaction. The particulate product from the reactor is then cooled in a cooler that is several times the reactor length.

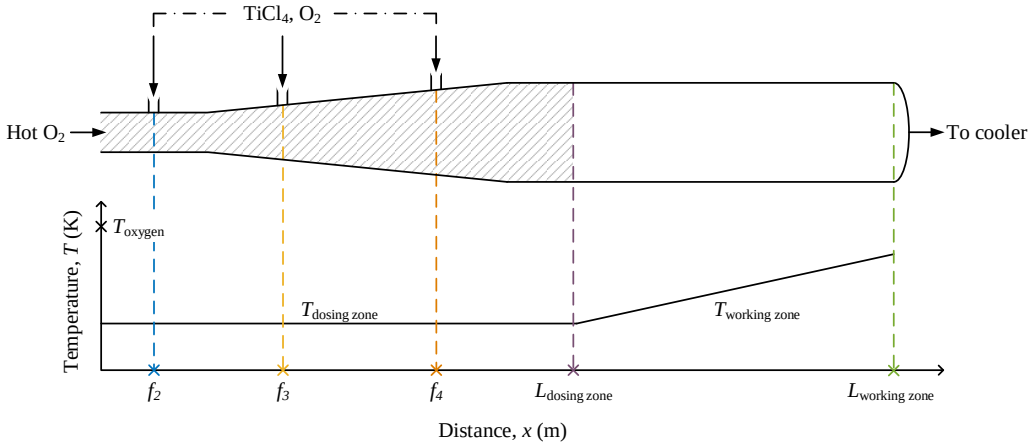

Figure 3: *Schematic of industrial titania reactor showing rough axial temperature profile and location of each feed stage relative to the reactor length L (not to scale), $L = L_{dosing\ zone} + L_{working\ zone}$. The labels f_2, f_3, f_4 designate the feed points.*

An ideal reactor network (**Figure 4**) is used to account for the axial variation in composition and temperature, while keeping the flow model simple enough to use a detailed particle model. This consists of a linear sequence of eleven CSTRs and two PFRs. The continuously stirred tank reactors are used as a dynamic model of the reactor dosing zone because good mixing is assumed to occur near the dosing points. Fresh $TiCl_4$ and O_2 is injected to every third CSTR in the network, as shown in Figure 4. The injection streams have volumetric feed fractions f_2, f_3 and f_4 relative to the total volumetric inflow to the corresponding reactor. Plug flow reactors with prescribed positive and negative temperature gradients are used to model the reactor working zone and the cooler respectively.

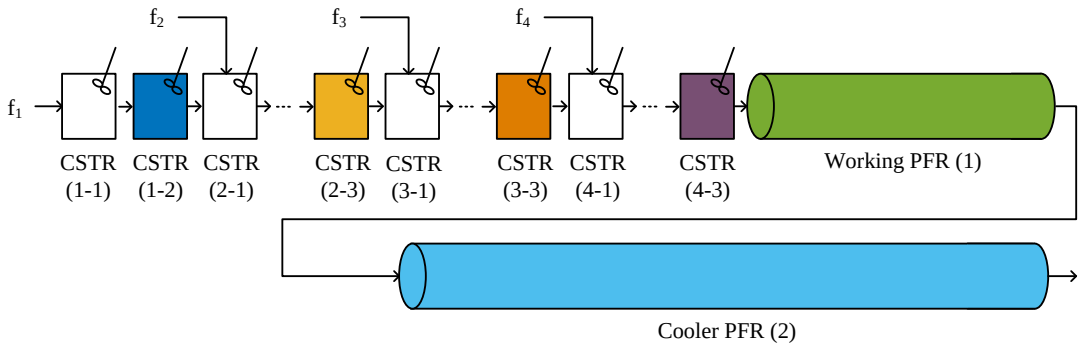

Figure 4: *Ideal reactor network with feed injection f_i to CSTR (i-1), i.e. the first reactor in the i^{th} section, $i = 1,\ldots,4$. Results will be shown for the final reactor in each section, i.e. CSTRs (1-2), (2-3), (3-3), (4-3) and for PFRs (1) and (2).*

Table 1: *Base case operating conditions in the reactor network. Zones are: D – dosing zone; W – working zone; C – cooling zone.*

Zone -	Reactor -	Feed fraction f (-)	Residence time τ (ms)	Temperature T (K)
D	CSTR (1-1)	1.0	2.0	1200
D	CSTR (1-2)	0	2.0	1200
D	CSTR (2-1)	0.50	5.0	1200
D	CSTR (2-2)	0	5.0	1200
D	CSTR (2-3)	0	5.0	1200
D	CSTR (3-1)	0.30	5.0	1200
D	CSTR (3-2)	0	5.0	1200
D	CSTR (3-3)	0	5.0	1200
D	CSTR (4-1)	0.40	5.0	1200
D	CSTR (4-2)	0	5.0	1200
D	CSTR (4-3)	0	5.0	1200
W	PFR (1)	0	160	1200-1600
C	PFR (2)	0	1500	1600-400

The base case operating conditions used in this work are listed in **Table 1**. Typical industrial conditions are used, such as an approximately equimolar ratio of $TiCl_4$ to O_2 in feeds f_2, f_3 and f_4 [3] and a pressure of around 4 bar. Feed f_1 is predominantly O_2 with a small amount of $TiCl_4$.

4 Results and discussion

The reactor network model is used to study the distributions of the size and structural characteristics of titania particles formed under industrial synthesis conditions. Particle growth is investigated in detail for a base case simulation in Section 4.1, with a brief discussion of numerical considerations in Section 4.1.2. In Section 4.2, a parameter study is used to compare the product size and structure resulting from different process conditions.

4.1 Base case

The evolution of the particle distributions under the base case conditions is shown in **Figure 5**. The characteristics chosen for study are the number of primaries per particle (Figure 5(a)), the mean collision and primary diameters (Figures 5(b),5(c)) and the mean neck radius (Figure 5(d)) for each aggregate. The mean value and the densities derived from a kernel estimator are included with the distributions to highlight the trends across the reactor-cooler. The Matlab *ksdensity* function [25] was used to fit the estimates based on a normal kernel function for the discrete simulation data, using the default adaptive bandwidth, and the fits were normalised to illustrate the number density. The fourth subfigure in each case compares the kernel estimators at the end of the reactor and cooler respectively.

Inception dominates near the beginning of the reactor due to the high reactant concentration and lack of particle surface area for surface reaction. Thus, most aggregates consist of one/several small primaries and have small collision diameters (Figure 5, CSTR (1-2)). The small mean neck radius indicates that most aggregated particles are in point contact. Further down the dosing zone, the distributions become increasingly broad as the particles become more polydisperse and more significantly connected (Figure 5, CSTR (4-3)).

Coagulation increases the mean collision diameters and number of primary particles of the particles. Surface growth increases the primary diameters and the neck radii become larger due to sintering between neighbouring primaries. Because coagulation is fast relative to sintering under the base case conditions, a significant proportion of the particles remains in point contact across the reactor (e.g. Figure 5(d), CSTR (4-3)).

In the working zone and cooler, the gas-phase precursor is depleted and there is no further change in mean primary diameter (Figure 5(c), PFR (1)). Coagulation and sintering continue, producing increasingly broad, flat distributions with large mean collision and neck diameters (Figures 5(a),5(b), 5(d) PFR (1)).

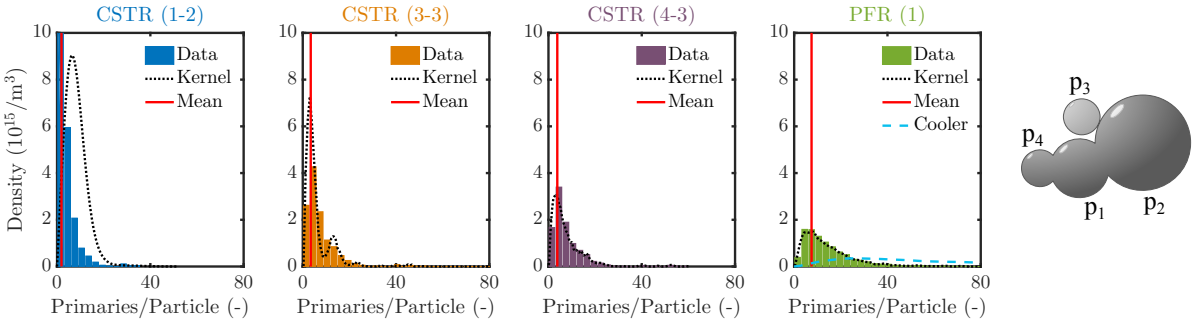

(a) Number of primaries per particle

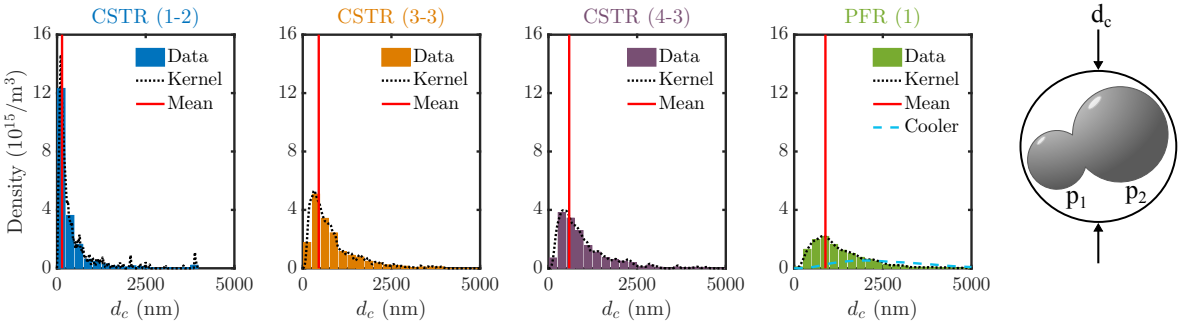

(b) Collision diameter, d_c

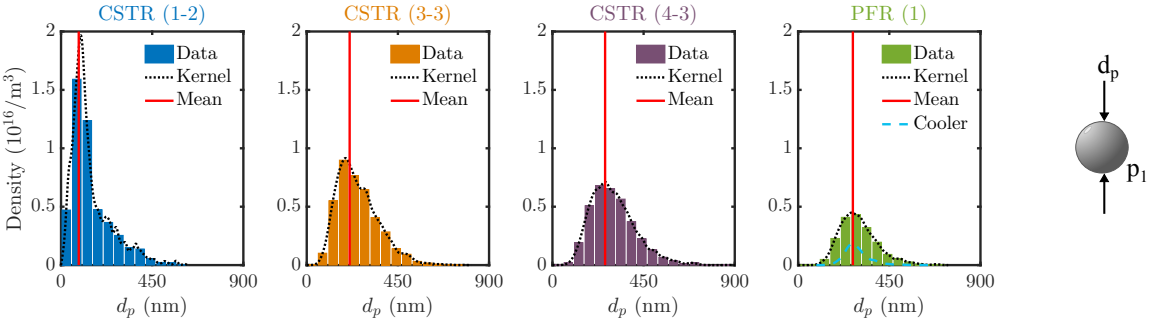

(c) Primary diameter, d_p

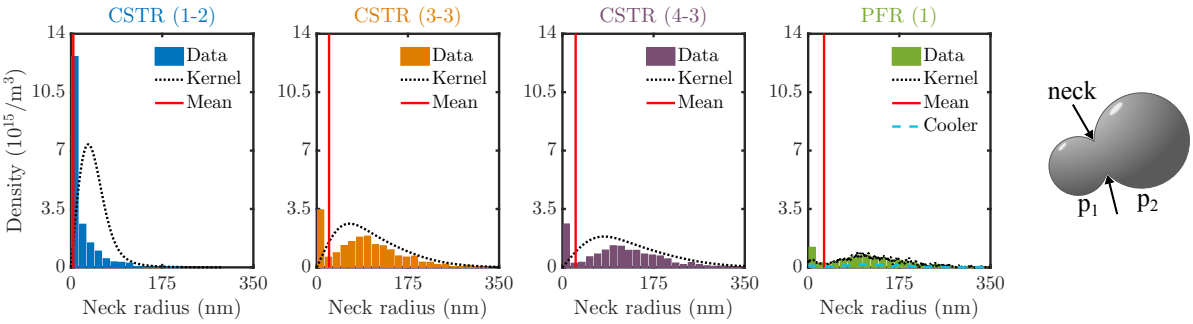

(d) Neck radius

Figure 5: *Raw simulation data, kernel density estimate and mean of the particle size distributions in CSTRs (1-2), (3-3), (4-3) and PFR (1); and kernel density estimate for PFR (2). Right-hand schematics illustrate each property.*

4.1.1 Transient evolution of particle properties

The transient evolution of the particle collision diameters is explored at times 0.05τ, 0.5τ, τ and 5τ ($\tau = 2$ ms) in CSTR (1-1). Lognormal kernel density estimates (Appendix A) for the collision diameter raw data are compared in **Figure 6**. At the early time, the distribution consists of a single peak, that is just larger than the incepting particle size (0.49 nm). For 0.5τ and τ, the mean of the distribution is increasingly large due to coagulation (increasing the particle collision diameter) and surface growth (indirectly contributing to a larger collision diameter by increasing the primary diameters). The absence of a peak at the incepting particle size (0.49 nm) suggests that coagulation is rapid, especially for the smallest particles. By 5τ, the steady-state has been established and this is observed to consist of a bimodal distribution, with a peak centred at the incepting particle size and a second peak at approximately 550 nm. These observations indicate that the characteristic time of the coagulation process is relatively short compared to the CSTR residence time.

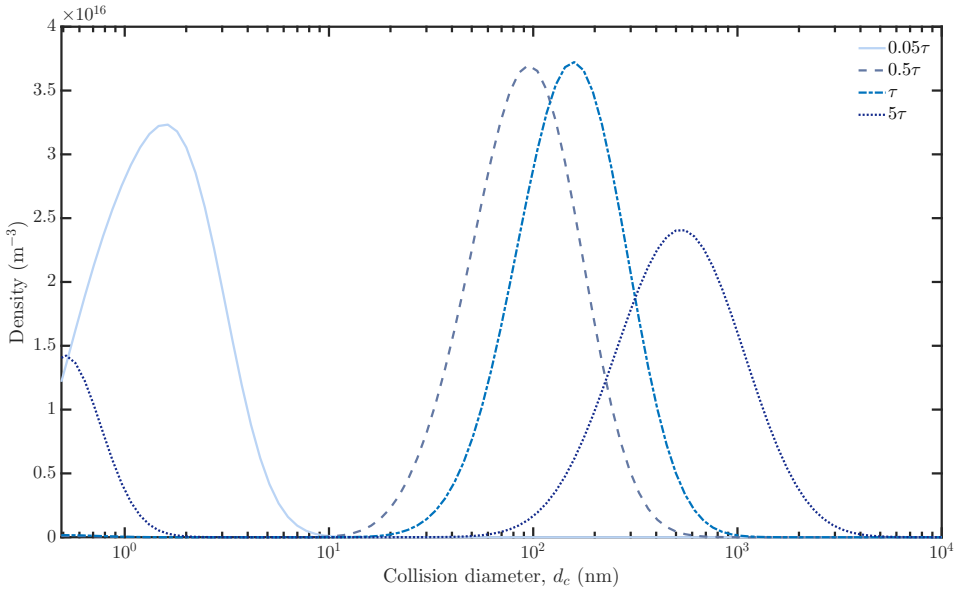

Figure 6: *Lognormal kernel estimates (with $\sigma = 0.4$) for the collision diameter simulation data, for four time points during transience in CSTR (1-1) with $\tau = 2$ ms. Extension below 0.49 nm is a consequence of the continuous smoothing kernel.*

4.1.2 Numerical considerations

The direct simulation algorithm was used to produce the results presented in this paper. The stochastic weighted algorithm was found to produce comparable statistical errors across the network. However, in contrast to a previous study for CSTR networks with recycles [29], SWA was not found to reduce the statistical error in the particle moments. This is because the current reactor network is linear. The run time with 2^{14} particles was approximately 33 hours (for DSA) on a 3 GHz Intel Xeon X5472 processor with 8 GB of

RAM, running 64-bit CentOS Linux 7.

The statistical error and convergence behaviour are considered for CSTR (2-1), under the base case simulation conditions, with DSA (**Figure 7**). The average relative statistical error, $\bar{\varepsilon}_{\text{stat}}$, is defined in Equation (12), where M is the number of time steps, N and R are the ensemble capacity and the number of repeats, and c_θ and μ_θ are the 99.9% confidence interval and the mean for the property θ [29].

$$\bar{\varepsilon}_{\theta,\text{stat}} = \frac{1}{M}\sum_{m=1}^{M}\frac{c_\theta^{(N,R)}(t_m)}{\mu_\theta^{(N,R)}(t_m)} \tag{12}$$

The particle moments used in this analysis are defined in Equation (13), where, w_i and $v^{(i)}$ are the relative weight and volume of the i^{th} particle and ρ is the mass density of TiO_2.

$$M_k(t) = \frac{1}{V_{\text{smp}}}\sum_{i=1}^{N(t)} w_i\left(\rho v^{(i)}\right)^k, \quad k = 0,1,2 \tag{13}$$

The statistical errors in the lower order particle moments, the collision diameter, the primary diameter and the number of primary particles per particle (n_p) are compared using $N^{(\max)} = 2^{14}$ computational particles and $R = 10$ repeat runs (Figure 7(a)). The statistical errors are observed to increase in the higher order moments as was found in other works [29, 38]. The statistical errors in properties that are of interest in this work are sufficiently low. Convergence as a function of the number of computational particles is shown for the particle and primary particle diameters and the first mass moment with $N^{(\max)} \times R = 2^{17}$ (Figure 7(b)). All properties are relatively level by $N^{(\max)} = 2^{14}$, the value used here.

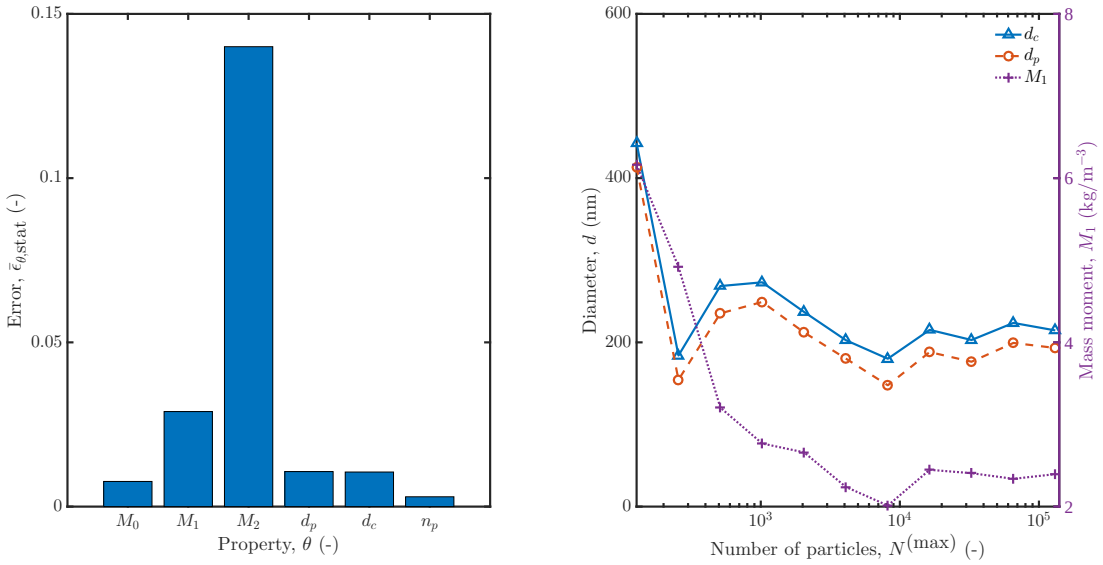

(a) Average relative statistical error

(b) Convergence behaviour

Figure 7: *Steady-state statistical error and convergence behaviour of the particle moments and the particle size characteristics in CSTR (2-1).*

4.2 Preliminary sensitivity study

The effect of changing reactor configuration and operating conditions on the particle properties is explored in this section to demonstrate the potential to use the detailed model to understand the process and important parameters. Three reactor configurations (test cases 0, 1 and 2), two temperatures (test cases 0 and 3) and two residence times (test cases 0 and 4) were considered, as summarised in **Table 2**. The reactor configuration was changed by moving the location of the three feed sites as illustrated in **Figure 8**.

Table 2: *Operational parameters used in the base case (0) and test cases (1-4) varying the feed injection points, temperature and flow rate.* $\{\tau\}_{bc}$ *is the set of base case residence times.*

Case -	Temperature T, K	2nd feed CSTR #	3rd feed CSTR #	4th feed CSTR #	Residence time $\{\tau\}$, ms
0	1200	3	6	9	$1 \times \{\tau\}_{bc}$
1	1200	2	3	4	$1 \times \{\tau\}_{bc}$
2	1200	9	10	11	$1 \times \{\tau\}_{bc}$
3	1100	3	6	9	$1 \times \{\tau\}_{bc}$
4	1200	3	6	9	$\frac{1}{2} \times \{\tau\}_{bc}$

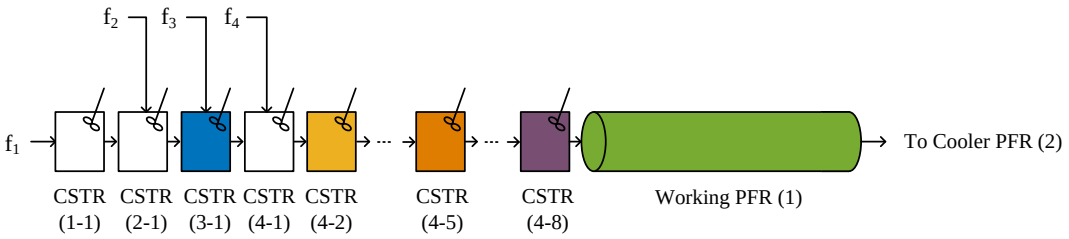

(a) Early dosage injection inlets (case 2)

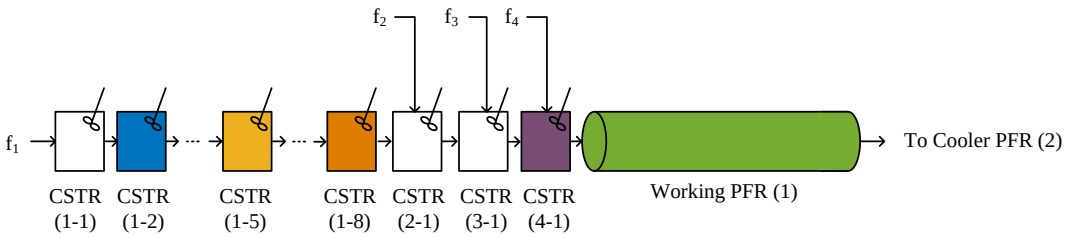

(b) Late dosage injection inlets (case 3)

Figure 8: *Reactor network configurations with different dosing points compared to the base case reactor dosing scheme, in which* f_2*,* f_3 *and* f_4 *were allocated to the third, sixth and ninth CSTRs respectively.*

The effect of temperature and residence time on the particle size and structure is summarised using the mean and geometric standard deviation of the aggregate and primary particle diameters, the number of primaries per particle and the number density (**Figure 9** and **Table 3**). These properties are chosen so as to accommodate qualitative comparison with literature studies and plant experience, in the absence of relevant data.

In the base case, particle inception dominates near the reactor inlet, as can be seen from the preliminary spike in the number density in Figure 9. The surface reaction proceeds rapidly across the dosing zone, near the fresh feed points, and a sharp increase in the mean primary diameter is observed. The primary diameter remains almost constant in the reactor working zone and the cooler because the rate of the surface reaction is diminished at the significantly lower reactant concentrations there. The final mean primary diameter is 277 nm.

Coagulation occurs throughout the reactor and cooler, as can be seen in the increasing collision diameter and decreasing particle number density, as well as the aggregate structure shown in the simulated TEMs, in Figure 9. The final product consists of particles with a mean size of 2000 nm, comprised of on average 32 primary particles per particle, with a mean neck radius of 38 nm, indicating partial sintering between neighbouring connected primary particles.

Increasing the reactor temperature increased the mean collision diameter and decreased the mean primary diameter and number density. These trends are indicated with dashed arrows in Figure 9 and can be explained by comparing the relative rates of the different processes at different temperatures. The particle process rates are greater at higher temperatures; however, the effect of temperature on the inception and coagulation rates is relatively large compared to the effect on the surface growth rate.

Akhtar et al. [1] used an aerosol reactor to investigate the effect of temperature in the range 1200-1723 K. The particle size distribution was found to shift to larger particle sizes with increased temperature and a theoretical study showed an increase in coagulation. As in the current work, there was little change in the geometric standard deviation (Table 3). Nakaso et al. [30] also observed that, for temperatures in the range studied here, higher temperatures produced larger particles consisting of smaller primaries, and lower temperatures resulted in less dense aggregates of larger primaries. Other studies also report this effect [54]. The primary diameter might begin to increase again for temperatures higher than the ones investigated here due to complete sintering between primary particles [30].

Increasing the flow rate produced smaller primary and aggregate particles (indicated with dashed arrows in Figure 9), and a higher number density because the particles had less time to grow. Again, this is supported by the trend reported in the literature [1] and this finding also agrees with empirical experience of the industrial process.

In this work, the same base case temperature profile was used for the early and late dosing cases. This is sufficient for the current study; however, the choice of dosing configuration is complex, since it affects the concentration profile and temperature exotherm. It would be useful to adjust the temperature profile to match the dosing strategy to account for the change in temperature due to the reaction. Here, the early dosing configuration created slightly smaller particles and a higher particle number concentration while the late dosing configuration produced significantly smaller primary particles (Table 3).

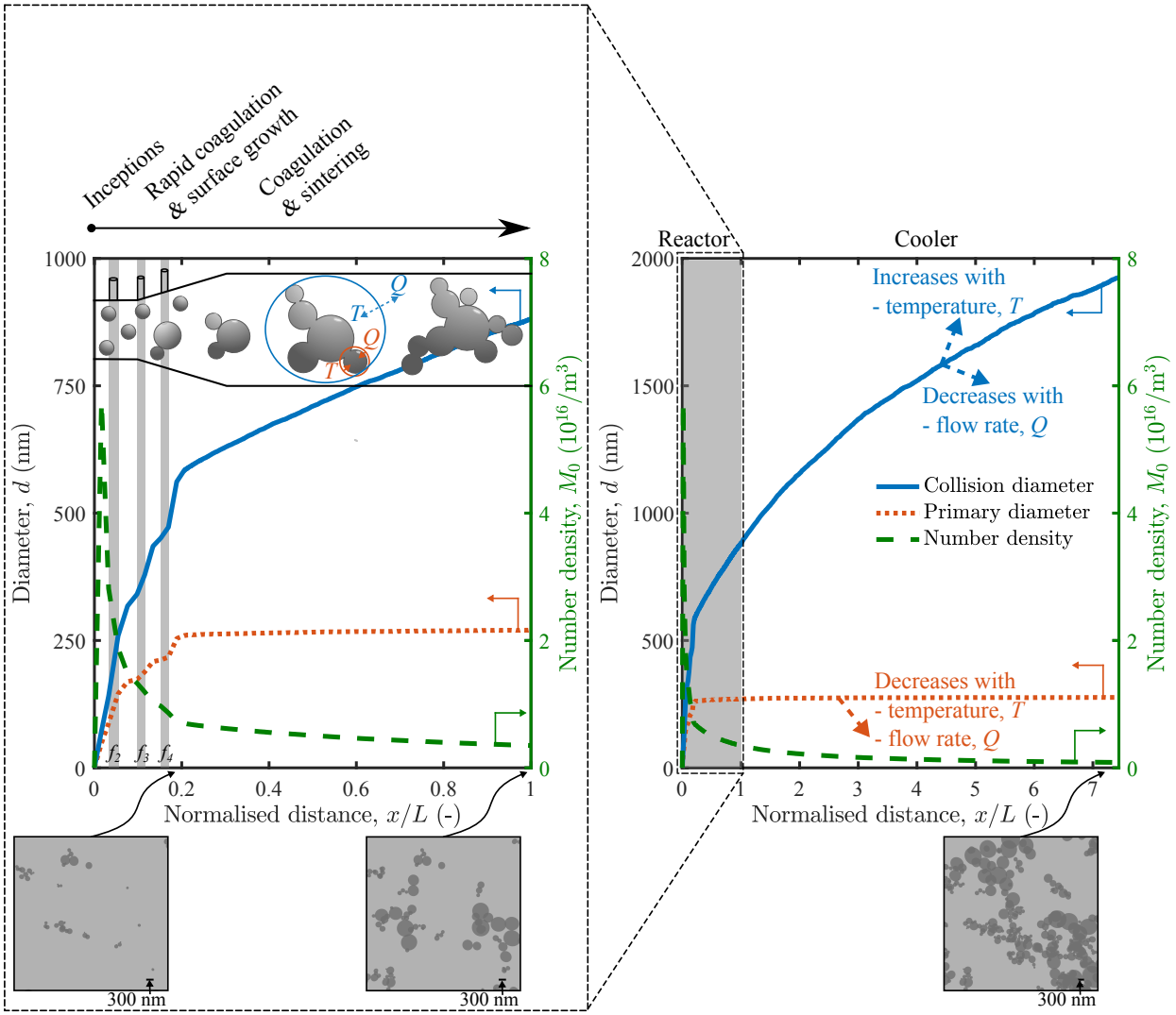

Figure 9: *Evolution of particle size and number density across the reactor and cooler (normalised by reactor length L) for the base conditions. Dashed arrows show the effects of increasing temperature T and throughout Q. The simulated TEM images were generated using the freeware ray tracing program POV-Ray to visualise the simulation surface data for the set of computational particles.*

A smaller mean particle size is desirable to reduce milling requirements. This short study suggests that the use of high throughput, with rapid quenching at the end of the working zone and in the cooler, is necessary to minimise coagulation and sintering of the pigmentary particles and thereby improve product quality with minimal requirement on milling.

Table 3: *Mean and geometric standard deviation (GSD, $\tilde{\sigma}$) of collision diameter and primary diameter and mean number density after the cooler for each case in Table 2.*

Test case	Mean	GSD	Mean	GSD	Mean
-	$\bar{d}_c$, nm	$\tilde{\sigma}_{d_c}$	$\bar{d}_p$, nm	$\tilde{\sigma}_{d_p}$	$\bar{M}_0$, m^{-3}
Base case	2000	1.79	277	1.23	8.14×10^{14}
Early dosage	1910	1.77	272	1.21	8.44×10^{14}
Late dosage	1990	1.77	246	1.27	8.07×10^{14}
Low temperature	1800	1.74	356	1.23	9.02×10^{14}
High throughput	1590	1.76	251	1.23	15.1×10^{14}

5 Conclusions

This paper has presented a model for titania synthesis in an industrial reactor. Important features include an ideal reactor network to treat the flow behaviour and describe variations in composition and temperature; and a detailed population balance to describe the particle system, coupled to a comprehensive chemical mechanism. The use of a detailed particle model allows for many internal co-ordinates of the particles to be tracked, and these are believed to provide important information about the aggregate structure. Aggregate size and morphology are critical factors in determining the product quality, which in turn impacts the milling requirement of the industrial process. It is thus believed to be useful to obtain as much information as possible about the particle aggregates.

In particular, the distributions of the number of primary particles per particle, collision diameter, primary particle diameter, and neck radius are tracked along the reactor-cooler. The pigmentary product leaving the cooler is shown to consist of partially sintered groups of connected primary particles, such that the particles are on average several times larger than their constituent primary particles. This has implications for the amount of milling that would be necessary to produce particles of the requisite size in the industrial process.

A preliminary sensitivity study found that increasing temperature resulted in the formation of larger particles, comprised of smaller primary particles, owing to the relative rates of the particle processes at different temperatures. This agrees with previous studies. Higher throughput produced smaller particles due to the limited time for reaction and particle growth. This is supported by empirical experience of the industrial process. Thus, although there is not currently industrial data to compare such trends quantitatively, the effects of operational changes were found to agree qualitatively with trends published for a number of laboratory studies.

This work serves as proof-of-concept for the use of a reactor network with a detailed pop-

ulation balance to simulate industrial titania synthesis. Avenues for future work could include development of a more detailed sintering model and inclusion of crystal structure information in the particle description. Regarding the latter, Xu et al. [52] have recently demonstrated such a phase-transformation model in a CFD-population balance Monte Carlo simulation for flame synthesis of TiO_2. A full sensitivity study could then be performed towards optimising the PSD; investigating temperature hot-spots, the effect of the $AlCl_3$ additive [43] and operational design limitations; and studying the parameters defining the particle processes. The Model Development Suite (MoDS) [8] software tool could be utilised to do this, and to fit cheaper surrogate models [12] to the simulation data.

Acknowledgements

This project is partly funded by the National Research Foundation (NRF), Prime Minister's Office, Singapore under its Campus for Research Excellence and Technological Enterprise (CREATE) programme. The authors would like to thank Huntsman Pigments and Additives for financial support.

Nomenclature

Upper-case Roman

A	Surface area	[m^2]
$\mathbf{C}$	Connectivity matrix	
E_a	Arrhenius activation energy	[$kJ \cdot mol^{-1}$]
K_{fm}	Free molecular regime coagulation kernel	
Kn	Knudsen number	
K_{sf}	Slip flow regime coagulation kernel	
K_{tr}	Transition regime coagulation kernel	
L	Length	[m]
M	Number of time steps	
M_0	0^{th} number moment	[m^{-3}]
M_k	k^{th} mass moment	[$kg^k \cdot m^{-3k}$]
N	Number of particles in the ensemble	
P	Pressure	[bar]
$\mathbf{P}$	Probability	
P	Particle	
Q	System state	
R	Gas constant	[$m^3 \cdot bar \cdot K^{-1} \cdot mol^{-1}$]
R	Number of repeat runs	
T	Temperature	[K]

V	Volume	[m^3]
V_{smp}	Sample volume	[m^3]

Lower-case Roman

c	Confidence interval (here 99.9%)	
d_c	Collision diameter	[nm]
d_p	Primary particle diameter	[nm]
f	Volumetric feed fraction	
k_B	Boltzmann constant	[$J \cdot K^{-1}$]
k_s	Surface growth rate constant, Arrhenius form	[$m^4 \cdot s^{-1} \cdot mol^{-1}$]
k_1	Arrhenius constant	[$m^4 \cdot s^{-1} \cdot mol^{-1}$]
m	Mass	[kg]
n	Number of primary particles	
p	Primary particle	
t	Time	[s]
v	Primary particle volume	[m^3]
w	Statistical weight	
x	Axial distance	[m]

Lower-case Greek

$\bar{\varepsilon}_{stat}$	Average relative statistical error	
η	Number of elements	
θ	Property	
μ	Mean	
ρ	Mass/molar density (specified in the text)	[$kg \cdot m^{-3}$]/[$mol \cdot m^{-3}$]
σ	Standard deviation	
$\tilde{\sigma}$	Geometric standard deviation	
τ	Residence time	[s]
τ_c	Characteristic sintering time	[s]

Superscripts

max	Maximum
sph	Sphere (denotes property of a mass equivalent sphere)

Subscripts

bc	Base case
i	Index variable
j	Index variable
k	Index variable
0	Denotes the number zero – added to the set of natural numbers

Symbols

$\mathbb{N}$	Set of natural numbers

Abbreviations

CFD	Computational fluid dynamics
CSTR	Continuous stirred tank reactor
DSA	Direct simulation algorithm
PFR	Plug flow reactor
PSD	Particle size distribution
SWA	Stochastic weighted algorithm
TEM	Transmission electron microscopy
MoDS	Model Development Suite

References

[1] M. K. Akhtar, Y. Xiong, and S. E. Pratsinis. Vapor synthesis of titania powder by titanium tetrachloride oxidation. *Journal of Aerosol Science*, 22(SUPPL. 1):S35–S38, 1991. ISSN 00218502. doi:10.1016/S0021-8502(05)80028-X.

[2] M. K. Akhtar, G. G. Lipscomb, and S. E. Pratsinis. Monte Carlo Simulation of Particle Coagulation and Sintering. *Aerosol Science and Technology*, 21(1):83–93, 1994. ISSN 0278-6826. doi:10.1080/02786829408959698.

[3] J. Akroyd, A. J. Smith, R. Shirley, L. R. McGlashan, and M. Kraft. A coupled CFD-population balance approach for nanoparticle synthesis in turbulent reacting flows. *Chemical Engineering Science*, 66(17):3792–3805, 2011. ISSN 00092509. doi:10.1016/j.ces.2011.05.006.

[4] C. Artelt, H. J. Schmid, and W. Peukert. Modelling titania formation at typical industrial process conditions: effect of surface shielding and surface energy on relevant growth mechanisms. *Chemical Engineering Science*, 61(1):18–32, 2006. ISSN 00092509. doi:10.1016/j.ces.2004.12.053.

[5] M. Balthasar, F. Mauss, A. Knobel, and M. Kraft. Detailed modeling of soot formation in a partially stirred plug flow reactor. *Combustion and Flame*, 128(4):395–409, 2002. ISSN 00102180. doi:10.1016/S0010-2180(01)00344-3.

[6] M. Celnik, R. I. A. Patterson, M. Kraft, and W. Wagner. Coupling a stochastic soot population balance to gas-phase chemistry using operator splitting. *Combustion and Flame*, 148(3):158–176, 2007. ISSN 00102180. doi:10.1016/j.combustflame.2006.10.007.

[7] X. Chen and S. S. Mao. Titanium Dioxide Nanomaterials: Synthesis, Properties, Modifications, and Applications. *Chemical Reviews*, 107(7):2891–2959, 2007. ISSN 0009-2665. doi:10.1021/cr0500535.

[8] CMCL Innovations. MoDS (Model Development Suite), 2016. URL `http://www.cmclinnovations.com/mods/`. Accessed: 2016-11-05.

[9] A. Eibeck and W. Wagner. An Efficient Stochastic Algorithm for Studying Coagulation Dynamics and Gelation Phenomena. *SIAM Journal on Scientific Computing*, 22(3):802–821, 2000. ISSN 1064-8275. doi:10.1137/S1064827599353488.

[10] A. Eibeck and W. Wagner. Stochastic Particle Approximations for Smoluchoski's Coagualtion Equation. *The Annals of Applied Probability*, 11(4):1137–1165, 2001. ISSN 10505164. doi:10.1214/aoap/1015345398.

[11] A. Eibeck and W. Wagner. Stochastic interacting particle systems and nonlinear kinetic equations. *The Annals of Applied Probability*, 13(3):845–889, 2003. ISSN 1050-5164. doi:10.1214/aoap/1060202829.

[12] A. I. J. Forrester, A. Sóbester, and A. J. Keane. *Engineering Design via Surrogate Modelling: A Practical Guide*. John Wiley & Sons, Chichester, UK, 2008. ISBN 9780470770801. doi:10.1002/9780470770801.

[13] M. Frenklach and S. J. Harris. Aerosol dynamics modeling using the method of moments. *Journal of Colloid and Interface Science*, 118(1):252–261, 1987. ISSN 00219797. doi:10.1016/0021-9797(87)90454-1.

[14] S. C. Garrick and G. Wang. Modeling and simulation of titanium dioxide nanoparticle synthesis with finite-rate sintering in planar jets. *Journal of Nanoparticle Research*, 13(3):973–984, 2011. ISSN 1388-0764. doi:10.1007/s11051-010-0097-x.

[15] M. J. Gázquez, J. P. Bolívar, R. Garcia-Tenorio, and F. Vaca. A Review of the Production Cycle of Titanium Dioxide Pigment. *Materials Sciences and Applications*, 05(07):441–458, 2014. ISSN 2153-117X. doi:10.4236/msa.2014.57048.

[16] A. P. George, R. D. Murley, and E. R. Place. Formation of TiO_2 aerosol from the combustion supported reaction of $TiCl_4$ and O_2. *Faraday Symposia of the Chemical Society*, 7:63, 1973. ISSN 0301-5696. doi:10.1039/fs9730700063.

[17] R. N. Ghoshtagore. Mechanism of Heterogeneous Deposition of Thin Film Rutile. *Journal of The Electrochemical Society*, 117(4):529, 1970. ISSN 00134651. doi:10.1149/1.2407561.

[18] E. Goudeli, M. L. Eggersdorfer, and S. E. Pratsinis. Aggregate characteristics accounting for the evolving fractal-like structure during coagulation and sintering. *Journal of Aerosol Science*, 89:58–68, 2015. ISSN 00218502. doi:10.1016/j.jaerosci.2015.06.008.

[19] R. Hong, Z. Ren, J. Ding, and H. Li. Experimental investigation and particle dynamic simulation for synthesizing titania nanoparticles using diffusion flame. *Chemical Engineering Journal*, 108(3):203–212, 2005. ISSN 13858947. doi:10.1016/j.cej.2005.02.011.

[20] E. V. Kartaev, V. P. Lukashov, S. P. Vashenko, S. M. Aulchenko, O. B. Kovalev, and D. V. Sergachev. An Experimental Study of the Synthesis of Ultrafine Titania Powder in Plasmachemical Flow-Type Reactor. *International Journal of Chemical Reactor Engineering*, 12(1):377–396, 2014. ISSN 2194-5748. doi:10.1515/ijcre-2014-0001.

[21] A. Kobata, K. Kusakabe, and S. Morooka. Growth and transformation of TiO_2 crystallites in aerosol reactor. *AIChE Journal*, 37(3):347–359, 1991. ISSN 0001-1541. doi:10.1002/aic.690370305.

[22] W. Koch and S. Friedlander. The effect of particle coalescence on the surface area of a coagulating aerosol. *Journal of Colloid and Interface Science*, 140(2):419–427, 1990. ISSN 00219797. doi:10.1016/0021-9797(90)90362-R.

[23] M. Kraft. Modelling of Particulate Processes. *KONA Powder and Particle Journal*, 23(March):18–35, 2005. ISSN 0288-4534. doi:10.14356/kona.2005007.

[24] F. E. Kruis, K. A. Kusters, S. E. Pratsinis, and B. Scarlett. A Simple Model for the Evolution of the Characteristics of Aggregate Particles Undergoing Coagulation and Sintering. *Aerosol Science and Technology*, 19(4):514–526, 1993. ISSN 0278-6826. doi:10.1080/02786829308959656.

[25] MathWorks. R2016a Documentation: 'ksdensity', Kernel smoothing function estimate for univariate and bivariate data, 2016. URL https://www.mathworks.com/help/stats/ksdensity.html?searchHighlight=ksdensity. Accessed: 2016-11-09.

[26] M. Mehta, Y. Sung, V. Raman, and R. O. Fox. Multiscale Modeling of TiO_2 Nanoparticle Production in Flame Reactors: Effect of Chemical Mechanism. *Industrial & Engineering Chemistry Research*, 49(21):10663–10673, 2010. ISSN 0888-5885. doi:10.1021/ie100560h.

[27] M. Mehta, V. Raman, and R. O. Fox. On the role of gas-phase and surface chemistry in the production of titania nanoparticles in turbulent flames. *Chemical Engineering Science*, 104(2013):1003–1018, 2013. ISSN 00092509. doi:10.1016/j.ces.2013.10.039.

[28] W. J. Menz and M. Kraft. The Suitability of Particle Models in Capturing Aggregate Structure and Polydispersity. *Aerosol Science and Technology*, 47(7):734–745, 2013. ISSN 0278-6826. doi:10.1080/02786826.2013.788244.

[29] W. J. Menz, J. Akroyd, and M. Kraft. Stochastic solution of population balance equations for reactor networks. *Journal of Computational Physics*, 256:615–629, 2014. ISSN 00219991. doi:10.1016/j.jcp.2013.09.021.

[30] K. Nakaso, K. Okuyama, M. Shimada, and S. E. Pratsinis. Effect of reaction temperature on CVD-made TiO_2 primary particle diameter. *Chemical Engineering Science*, 58(15):3327–3335, 2003. ISSN 00092509. doi:10.1016/S0009-2509(03)00213-6.

[31] I. V. Novosselov and P. C. Malte. Development and Application of an Eight-Step Global Mechanism for CFD and CRN Simulations of Lean-Premixed Combustors. *Journal of Engineering for Gas Turbines and Power*, 130(2):021502, 2008. ISSN 07424795. doi:10.1115/1.2795787.

[32] I. V. Novosselov, P. C. Malte, S. Yuan, R. Srinivasan, and J. C. Y. Lee. Chemical Reactor Network Application to Emissions Prediction for Industial DLE Gas Turbine. In *Volume 1: Combustion and Fuels, Education*, volume 2006, pages 221–235. ASME, 2006. ISBN 0-7918-4236-3. doi:10.1115/GT2006-90282.

[33] H. K. Park and K. Y. Park. Control of Particle Morphology and Size in Vapor-Phase Synthesis of Titania, Silica and Alumina Nanoparticles. *KONA Powder and Particle Journal*, 32(32):85–101, 2015. ISSN 0288-4534. doi:10.14356/kona.2015018.

[34] R. I. A. Patterson. Convergence of Stochastic Particle Systems Undergoing Advection and Coagulation. *Stochastic Analysis and Applications*, 31(5):800–829, 2013. ISSN 0736-2994. doi:10.1080/07362994.2013.817245.

[35] R. I. A. Patterson. Properties of the solutions of delocalised coagulation and inception problems with outflow boundaries. *Journal of Evolution Equations*, 16(2): 261–291, 2016. ISSN 1424-3199. doi:10.1007/s00028-015-0302-6.

[36] R. I. A. Patterson and M. Kraft. Models for the aggregate structure of soot particles. *Combustion and Flame*, 151(1-2):160–172, 2007. ISSN 00102180. doi:10.1016/j.combustflame.2007.04.012.

[37] R. I. A. Patterson, J. Singh, M. Balthasar, M. Kraft, and J. R. Norris. The Linear Process Deferment Algorithm: A new technique for solving population balance equations. *SIAM Journal on Scientific Computing*, 28(1):303–320, 2006. ISSN 1064-8275. doi:10.1137/040618953.

[38] R. I. A. Patterson, W. Wagner, and M. Kraft. Stochastic weighted particle methods for population balance equations. *Journal of Computational Physics*, 230(19):7456–7472, 2011. ISSN 00219991. doi:10.1016/j.jcp.2011.06.011.

[39] S. E. Pratsinis and P. T. Spicer. Competition between gas phase and surface oxidation of $TiCl_4$ during synthesis of TiO_2 particles. *Chemical Engineering Science*, 53(10): 1861–1868, 1998. ISSN 00092509. doi:10.1016/S0009-2509(98)00026-8.

[40] S. E. Pratsinis, H. Bai, P. Biswas, M. Frenklach, and S. V. R. Mastrangelo. Kinetics of Titanium(IV) Chloride Oxidation. *Journal of the American Ceramic Society*, 73 (7):2158–2162, 1990. ISSN 0002-7820. doi:10.1111/j.1151-2916.1990.tb05295.x.

[41] M. Sander, R. H. West, M. S. Celnik, and M. Kraft. A Detailed Model for the Sintering of Polydispersed Nanoparticle Agglomerates. *Aerosol Science and Technology*, 43(10):978–989, 2009. ISSN 0278-6826. doi:10.1080/02786820903092416.

[42] S. Shekar, W. J. Menz, A. J. Smith, M. Kraft, and W. Wagner. On a multivariate population balance model to describe the structure and composition of silica nanoparticles. *Computers & Chemical Engineering*, 43:130–147, 2012. ISSN 00981354. doi:10.1016/j.compchemeng.2012.04.010.

[43] R. Shirley, Y. Liu, T. S. Totton, R. H. West, and M. Kraft. First-Principles Thermochemistry for the Combustion of a $TiCl_4$ and $AlCl_3$ Mixture. *The Journal of Physical Chemistry A*, 113(49):13790–13796, 2009. ISSN 1089-5639. doi:10.1021/jp905244w.

[44] P. T. Spicer, O. Chaoul, S. Tsantilis, and S. E. Pratsinis. Titania formation by $TiCl_4$ gas phase oxidation, surface growth and coagulation. *Journal of Aerosol Science*, 33 (1):17–34, 2002. ISSN 00218502. doi:10.1016/S0021-8502(01)00069-6.

[45] S. Tsantilis and S. E. Pratsinis. Evolution of primary and aggregate particle-size distributions by coagulation and sintering. *AIChE Journal*, 46(2):407–415, 2000. ISSN 00011541. doi:10.1002/aic.690460218.

[46] S. Tsantilis, H. Kammler, and S. Pratsinis. Population balance modeling of flame synthesis of titania nanoparticles. *Chemical Engineering Science*, 57(12):2139–2156, 2002. ISSN 00092509. doi:10.1016/S0009-2509(02)00107-0.

[47] C. G. Wells. A stochastic approximation scheme and convergence theorem for particle interactions with perfectly reflecting boundary conditions. *Monte Carlo Methods and Applications*, 12(3):291–342, 2006. ISSN 0929-9629. doi:10.1515/156939606778705182.

[48] R. H. West, G. J. O. Beran, W. H. Green, and M. Kraft. First-Principles Thermochemistry for the Production of TiO_2 from $TiCl_4$. *The Journal of Physical Chemistry A*, 111(18):3560–3565, 2007. ISSN 1089-5639. doi:10.1021/jp0661950.

[49] R. H. West, R. A. Shirley, M. Kraft, C. F. Goldsmith, and W. H. Green. A detailed kinetic model for combustion synthesis of titania from $TiCl_4$. *Combustion and Flame*, 156(9):1764–1770, 2009. ISSN 00102180. doi:10.1016/j.combustflame.2009.04.011.

[50] Y. Xiong and S. E. Pratsinis. Gas phase production of particles in reactive turbulent flows. *Journal of Aerosol Science*, 22(5):637–655, 1991. ISSN 00218502. doi:10.1016/0021-8502(91)90017-C.

[51] Y. Xiong and S. E. Pratsinis. Formation of agglomerate particles by coagulation and sintering – Part I. A two-dimensional solution of the population balance equation. *Journal of Aerosol Science*, 24(3):283–300, 1993. ISSN 00218502. doi:10.1016/0021-8502(93)90003-R.

[52] Z. Xu, H. Zhao, and H. Zhao. CFD-population balance Monte Carlo simulation and numerical optimization for flame synthesis of TiO_2 nanoparticles. *Proceedings of the Combustion Institute*, 000:1–10, 2016. ISSN 15407489. doi:10.1016/j.proci.2016.07.008.

[53] E. K. Yapp, R. I. A. Patterson, J. Akroyd, S. Mosbach, E. M. Adkins, J. Houston Miller, and M. Kraft. Numerical simulation and parametric sensitivity study of optical band gap in a laminar co-flow ethylene diffusion flame. *Combustion and Flame*, 167:320–334, 2016. ISSN 00102180. doi:10.1016/j.combustflame.2016.01.033.

[54] E. Zhou, Z.-F. Yuan, Z. Wang, X.-G. Fang, and J.-Z. Gong. Mechanism of scaling on oxidation reactor wall in TiO_2 synthesis by chloride process. *Transactions of Nonferrous Metals Society of China*, 16(2):426–431, 2006. ISSN 10036326. doi:10.1016/S1003-6326(06)60073-3.

A Particle size distributions

The probability density function of the collision diameter, $f(d_c)$, is estimated as the sum of log-normal distributions (for N stochastic particles in sample volume V_{smp}):

$$f(d_c) = \frac{1}{N}\sum_{n=1}^{N} \frac{1}{d_c \sigma \sqrt{2\pi}} \exp\left(-\frac{\left(\ln(d_c) - \ln\left(d_c^{(n)}\right)\right)^2}{2\sigma^2} \right) \tag{A.1}$$

Here, $d_c^{(n)}$ is the collision diameter of the n^{th} particle and σ is the standard deviation of the distribution, a parameter which can be modified in order to control the degree of smoothing. The number density is given by

$$g(d_c) = \frac{dn}{d(d_c)} = \frac{N}{V_{smp}} f(d_c) \tag{A.2}$$

and, from this,

$$\frac{dn}{d\ln(d_c)} = d_c \frac{dn}{d(d_c)} = d_c g(d_c) \tag{A.3}$$

B Numerical Methods

Algorithm B.1: Coupled reactor network with Strang splitting routine [29].

Input: Initial state Q_0 at t_0, final time t_f, time-step Δt, number of reactors n_{reac}
Output: Final state Q_f at t_f
Set $t \leftarrow t_0$, $Q \leftarrow Q_0$, $i_{reac} \leftarrow 1$
while $t < t_f$ **do**
  while $i_{reac} < n_{reac} + 1$ **do**
    Solve gas-phase chemistry for $\left[t, t + \frac{\Delta t}{2}\right]$.
    Solve particle-phase for $[t, t + \Delta t]$.
    Solve gas-phase chemistry for $\left[t + \frac{\Delta t}{2}, t + \Delta t\right]$.
    Increment $i_{reac} \leftarrow i_{reac} + 1$.
  end
  Increment $t \leftarrow t + \Delta t$.
end

Algorithm B.3: Direct Simulation Algorithm (DSA) with inflow/outflow [29, 42]

Input: Initial state Q_0 at t_0, final time t_f
Output: Final state Q_f at t_f
Set $t \leftarrow t_0$, $Q \leftarrow Q_0$
while $t < t_f$ **do**
Generate an exponentially distributed waiting time τ with parameter $R_{\text{total}}(Q)$:

$$R_{\text{total}}(Q) = R_{\text{inception}}(Q) + R_{\text{coagulation}}(Q) + R_{\text{surface}}(Q) + R_{\text{inflow}}(Q). \tag{B.1}$$

Choose process $\in$ {inception, surface, coagulation, inflow} with probability:

$$\mathbf{P}(\text{process}) = \frac{R_{\text{process}}(Q)}{R_{\text{total}}(Q)}. \tag{B.2}$$

if *process* = *inception* **then**
Perform inception by adding a new particle p_{N+1} to the ensemble.
else if *process* = *coagulation* **then**
Uniformly select two particles p_i, p_j, perform any tagged deferred events and then perform successful coagulation with probability:

$$\mathbf{P}_{i,j} = \frac{K_{\text{tr}}(p_i, p_j)}{\hat{K}(p_i, p_j)} \tag{B.3}$$

where K_{tr} is the transition regime kernel and $\hat{K}$ is the majorant kernel.
else if *process* = *surface* **then**
Uniformly select a particle p_i.
if *defer* = *true* **then**
Tag p_i for deferred surface reaction.
else
Perform surface reaction on p_i.
end
else if *process* = *inflow* **then**
Uniformly select a particle p_i and add N_{in} copies to the ensemble where:

$$N_{\text{in}} = \frac{V_{\text{smp}}}{V_{\text{smp}}^{(j)}}. \tag{B.4}$$

Here, V_{smp} and $V_{\text{smp}}^{(j)}$ are the current and inflow scaling factors.
end
Perform continuous outflow and sintering for $[t, t+\tau]$ and rescale the sample volume (τ_{CSTR} is the reactor residence time):

$$V_{\text{smp}}^{\text{new}} = \frac{V_{\text{smp}}}{1 - \tau/\tau_{\text{CSTR}}}. \tag{B.5}$$

Increment $t \leftarrow t + \tau$.
end
Perform outstanding deferred processes.